Follow the curvature of viscoelastic stress: Insights into the steady arrowhead structure

Pierre-Yves Goffin,[1] Yves Dubief,[2] and Vincent E. Terrapon[1,*]

[1]*Department of Aerospace and Mechanical Engineering, University of Liège, Liège, Belgium*
[2]*School of Engineering, University of Vermont, Vermont 05405, USA*

(Dated: May 21, 2026)

Here we provide an assessment of the accuracy of the numerical solution in Sec. I, decompose the polymer body force into its components along the principal stress directions in Sec. II, and derive and illustrate the interface jump conditions associated with the infinitesimal sheets approximation in Sec. III.

I. SOLUTION ACCURACY

The procedure for assessing the convergence to steady state was to compute the norm of the time derivative of the velocity and polymer fields, with sufficiently small values of those norms being indicative of temporal convergence. These time derivatives can be computed by evaluating the "residuals" of the momentum and polymer equations (Eqs. (2-3) in the main text). The L_2-norms of the time derivatives were then computed as

$$\langle \partial_t f \rangle_{\mathrm{L}_2} = \sqrt{\iint_\Omega (\partial_t f)^2 \,\mathrm{d}V}\,, \tag{1}$$

where f is a general solution field and Ω represents the two-dimensional domain described in the main text. We made use of Dedalus [1] differentiation and integration capabilities in order to ensure compatibility with the spectral discretization of the equations. Note that in general the polymer fields can be several orders of magnitude larger than the velocity fields and their respective residuals are thus expected to be accordingly higher. To compare them meaningfully, the polymer norms are all divided by L^2. We have computed $\langle \partial_t u \rangle_{\mathrm{L}_2} \approx 1.5\times10^{-9}$, $\langle \partial_t v \rangle_{\mathrm{L}_2} \approx 1.2\times10^{-11}$, $\langle \partial_t C_{xx}/L^2 \rangle_{\mathrm{L}_2} \approx 3.1\times10^{-10}$, $\langle \partial_t C_{yy}/L^2 \rangle_{\mathrm{L}_2} \approx 1.3\times10^{-12}$, $\langle \partial_t C_{zz}/L^2 \rangle_{\mathrm{L}_2} \approx 3.2\times10^{-14}$, $\langle \partial_t C_{xy}/L^2 \rangle_{\mathrm{L}_2} \approx 8.9\times10^{-11}$. These residuals are small enough for the solution to be considered as converged.

Additionally, Fig. S1 demonstrates that all spatial scales are resolved: for all fields and all wall normal positions considered, the highest resolved wavenumber corresponds to numerical noise. This proves that there is no energy accumulation at small scales. For completeness, the residual of the continuity condition has been computed as well and is $\langle \partial_x u + \partial_y v \rangle_{\mathrm{L}_2} \approx 3.4\times10^{-13}$, demonstrating the accuracy of the solution.

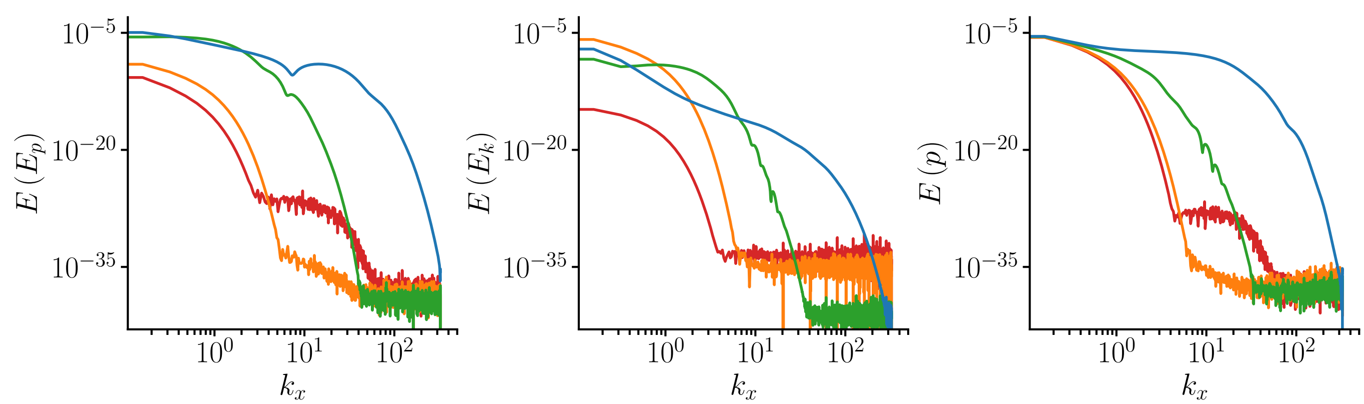

FIG. S1: Power spectra of different relevant fields computed along the streamwise direction and evaluated a different wall normal positions ($y = 0$ corresponds to the centerline and $y = 1$ corresponds to the upper wall): $y = 0$ (blue), $y = 0.2$ (green), $y = 0.8$ (orange) and $y = 1$ (red). From left to right: the elastic potential energy ($E_p = -\frac{1}{2}\frac{1-\beta}{Re\,Wi}L^2\ln(1-\frac{C_{kk}}{L^2})$), the kinetic energy ($E_k = \frac{1}{2}|\mathbf{u}|^2$) and the pressure fluctuation (p).

* Contact author: vincent.terrapon@uliege.be

II. POLYMER BODY FORCE DECOMPOSITION ALONG STRESSLINES

Introducing the index notations for the stress tensor in the general three-dimensional case

$$\tau_{ij} = \sum_{\alpha=1}^{3} \tau_\alpha e_i^{(\alpha)} e_j^{(\alpha)} , \tag{2}$$

where τ_α and $\mathbf{e}^{(\alpha)}$ are respectively the α-th eigenvalue and associated unit eigenvector, the polymer body force f_i is such that

$$\begin{aligned} \frac{Re}{1-\beta} f_i = \partial_j \tau_{ij} &= \sum_{\alpha=1}^{3} \left[e_i^{(\alpha)} e_j^{(\alpha)} \partial_j \tau_\alpha + \tau_\alpha e_i^{(\alpha)} \partial_j e_j^{(\alpha)} + \tau_\alpha e_j^{(\alpha)} \partial_j e_i^{(\alpha)} \right] \\ &= \sum_{\alpha=1}^{3} \left[e_i^{(\alpha)} \left(\tilde{\partial}_\alpha \tau_\alpha + \tau_\alpha \left(\boldsymbol{\nabla} \cdot \mathbf{e}^{(\alpha)} \right) \right) + \tau_\alpha \tilde{\partial}_\alpha e_i^{(\alpha)} \right] , \end{aligned} \tag{3}$$

where $\tilde{\partial}_\alpha = \mathbf{e}^{(\alpha)} \cdot \boldsymbol{\nabla}$ is the directional derivative in the direction $\mathbf{e}^{(\alpha)}$ and summation on repeated indices does not apply to index α.

A. Two-dimensional case

Focusing first on the specific two-dimensional case where the *dummy* direction is arbitrarily (but without loss of generality) chosen to be the 3$^{\text{rd}}$ one and introducing a general index basis $\{u, v\}$, we can use the geometrical definition of the curvature as follows:

$$\tilde{\partial}_u \mathbf{e}^{(u)} = \kappa_u \mathbf{e}^{(v)} \quad \Longrightarrow \quad \mathbf{e}^{(v)} \cdot \tilde{\partial}_u \mathbf{e}^{(u)} = \kappa_u , \tag{4}$$

where κ_u is the local curvature of the stressline $\boldsymbol{\mathcal{T}}_u$. As explained in the main text, we require $\mathbf{e}^{(v)}$ to point towards the local center of curvature of $\boldsymbol{\mathcal{T}}_u$ in order to define a positive curvature κ_v. It is also possible to show that the divergence of the eigenvectors is directly linked to curvature through

$$\boldsymbol{\nabla} \cdot \mathbf{e}^{(u)} = -\kappa_v . \tag{5}$$

We can project Eq. 3 onto $\mathbf{e}^{(u)}$ and, using the above results, we obtain

$$\begin{aligned} \frac{Re}{1-\beta} f_u &= \tilde{\partial}_u \tau_u - \tau_u \kappa_v + \tau_v \kappa_v , \\ &= \tilde{\partial}_u \tau_u - \kappa_v \left(\tau_u - \tau_v \right) , \end{aligned} \tag{6}$$

where $f_u = \mathbf{f} \cdot \mathbf{e}^{(u)}$. Considering that $N_1 = \tau_1 - \tau_2 \geq 0$ and replacing the indices as $\{u = 1, v = 2\}$ and $\{u = 2, v = 1\}$ we find

$$f_1 = \frac{1-\beta}{Re} \left(\tilde{\partial}_1 \tau_1 - \kappa_2 N_1 \right) , \quad f_2 = \frac{1-\beta}{Re} \left(\tilde{\partial}_2 \tau_2 + \kappa_1 N_1 \right) . \tag{7}$$

B. Three-dimensional case

Considering a general index basis $\{u, v, w\}$ for the three-dimensional case, we need to find expressions for the terms $\mathbf{e}^{(u)} \cdot \tilde{\partial}_v \mathbf{e}^{(v)}$ and $\boldsymbol{\nabla} \cdot \mathbf{e}^{(u)}$.

The first term is the definition of the normal curvature of a surface in the direction $\mathbf{e}^{(v)}$. The surface is the one generated by the tangent vectors $\{\mathbf{e}^{(v)}, \mathbf{e}^{(w)}\}$, denoted $S_{v,w}$ whose normal vector is $\mathbf{e}^{(u)}$. The normal curvature is denoted $\kappa_{v,w}^{(v)}$ where the indices $\cdot_{v,w}$ refer to the surface and $\cdot^{v}$ refers to the direction. Depending on the sign chosen for the normal $\mathbf{e}^{(u)}$, the normal curvature can be either positive or negative.

Another known result of differential geometry [2] is that $|\boldsymbol{\nabla} \cdot \mathbf{e}^{(u)}| = |2H_{v,w}|$, where $H_{v,w}$ is the mean curvature associated with the surface $S_{v,w}$. The difficulty is then to choose a preferred side for the normal $\mathbf{e}^{(u)}$ and assign the appropriate sign to the previous expression. In order to be *consistent* with the two-dimensional case derived above, we choose to orient the normal towards the convex side of $S_{v,w}$ if the surface is convex. In case of a *saddle surface* (considered here as a surface with negative Gaussian curvature), we orient the normal so that the normal curvature with the highest absolute value is positive. In doing so, we ensure the positivity of the mean curvature $H_{v,w} = (\kappa_{v,w}^{(v)} + \kappa_{v,w}^{(w)})/2$ such that $\boldsymbol{\nabla} \cdot \mathbf{e}^{(u)} = -2H_{v,w} = -\kappa_{v,w}^{(v)} - \kappa_{v,w}^{(w)}$.

Taking the dot product of Eq. 3 with $\mathbf{e}^{(u)}$ allows us to compute the expression of any component of the polymer body force:

$$\begin{aligned}\frac{Re}{1-\beta} f_u &= \tilde{\partial}_u \tau_u + \tau_u \left(\boldsymbol{\nabla} \cdot \mathbf{e}^{(u)}\right) + \sum_{\alpha=1}^{3} \tau_\alpha \mathbf{e}^{(u)} \cdot \tilde{\partial}_\alpha \mathbf{e}^{(\alpha)} \,, \\ &= \tilde{\partial}_u \tau_u + \tau_u \left(\boldsymbol{\nabla} \cdot \mathbf{e}^{(u)}\right) + \tau_v \mathbf{e}^{(u)} \cdot \tilde{\partial}_v \mathbf{e}^{(v)} + \tau_w \mathbf{e}^{(u)} \cdot \tilde{\partial}_w \mathbf{e}^{(w)} \,,\end{aligned} \tag{8}$$

where $f_u = \mathbf{f} \cdot \mathbf{e}^{(u)}$. The term $\alpha = u$ does not contribute to the sum as $\tilde{\partial}_u \mathbf{e}^{(u)}$ is orthogonal to $\mathbf{e}^{(u)}$. Injecting the previously derived expressions, we can write

$$\begin{aligned}\frac{Re}{1-\beta} f_u &= \tilde{\partial}_u \tau_u - \tau_u \left(\kappa_{v,w}^{(v)} + \kappa_{v,w}^{(w)}\right) + \tau_v \kappa_{v,w}^{(v)} + \tau_w \kappa_{v,w}^{(w)} \,, \\ &= \tilde{\partial}_u \tau_u - \kappa_{v,w}^{(v)} \left(\tau_u - \tau_v\right) - \kappa_{v,w}^{(w)} \left(\tau_u - \tau_w\right) \,.\end{aligned} \tag{9}$$

Replacing the indices as $\{u = 1, v = 2, w = 3\}$, $\{u = 2, v = 3, w = 1\}$ and $\{u = 3, v = 1, w = 2\}$ we find

$$\begin{cases} f_1 = \dfrac{1-\beta}{Re} \left[\tilde{\partial}_1 \tau_1 - \kappa_{2,3}^{(2)} \left(\tau_1 - \tau_2\right) - \kappa_{2,3}^{(3)} \left(\tau_1 - \tau_3\right)\right] \,, \\ f_2 = \dfrac{1-\beta}{Re} \left[\tilde{\partial}_2 \tau_2 + \kappa_{1,3}^{(1)} \left(\tau_1 - \tau_2\right) - \kappa_{1,3}^{(3)} \left(\tau_2 - \tau_3\right)\right] \,, \\ f_3 = \dfrac{1-\beta}{Re} \left[\tilde{\partial}_3 \tau_3 + \kappa_{1,2}^{(1)} \left(\tau_1 - \tau_3\right) + \kappa_{1,2}^{(2)} \left(\tau_2 - \tau_3\right)\right] \,. \end{cases} \tag{10}$$

The expressions have been reorganized so that, if we consider $\tau_1 \geq \tau_2 \geq \tau_3$, the terms inside the parentheses are positive and directly related to the first and second normal stress differences. The first two terms of the first two components are similar to the two-dimensional results except that in the general case the normal curvatures can be negative.

III. INTERFACE APPROXIMATION AND JUMP CONDITIONS

Considering the influence of the polymers to be localized on infinitesimally thin sheets and assuming a Newtonian fluid everywhere else, it is possible to derive stress jump conditions at those interfaces (akin to surface tension). Assuming two domains Ω_{I} and Ω_{II} separated by one interface Σ, whose unit normal $\mathbf{n}$ points towards Ω_{II}, the jump conditions write

$$\mathbf{T}_{\mathrm{II}} \cdot \mathbf{n} - \mathbf{T}_{\mathrm{I}} \cdot \mathbf{n} + \tilde{\mathbf{f}} = \mathbf{0} \,, \tag{11}$$

where $\mathbf{T}$ is the Newtonian stress tensor and $\tilde{\mathbf{f}}$ is the surface force distribution localized at the interface that represents the action of the polymers on the flow.

Decomposing the surface force into a normal and two tangential components (in 3D), the above conditions can be expressed as

$$\begin{cases} \mathbf{n} \cdot \mathbf{T}_{\mathrm{II}} \cdot \mathbf{n} - \mathbf{n} \cdot \mathbf{T}_{\mathrm{I}} \cdot \mathbf{n} = -\tilde{f}_n \,, \\ \mathbf{t_1} \cdot \mathbf{T}_{\mathrm{II}} \cdot \mathbf{n} - \mathbf{t_1} \cdot \mathbf{T}_{\mathrm{I}} \cdot \mathbf{n} = -\tilde{f}_{t_1} \,, \\ \mathbf{t_2} \cdot \mathbf{T}_{\mathrm{II}} \cdot \mathbf{n} - \mathbf{t_2} \cdot \mathbf{T}_{\mathrm{I}} \cdot \mathbf{n} = -\tilde{f}_{t_2} \,, \end{cases} \tag{12}$$

where $\tilde{f}_n$, $\tilde{f}_{t_1}$ and $\tilde{f}_{t_2}$ are the normal and tangential components of the surface force, respectively. Assuming the same Newtonian fluid in both domains, the conditions become

$$\begin{cases} p_{\mathrm{I}} - p_{\mathrm{II}} + 2\mu(\mathbf{n} \cdot \mathbf{E}_{\mathrm{II}} \cdot \mathbf{n} - \mathbf{n} \cdot \mathbf{E}_{\mathrm{I}} \cdot \mathbf{n}) = -\tilde{f}_n \,, \\ 2\mu(\mathbf{t_{1,2}} \cdot \mathbf{E}_{\mathrm{II}} \cdot \mathbf{n} - \mathbf{t_{1,2}} \cdot \mathbf{E}_{\mathrm{I}} \cdot \mathbf{n}) = -\tilde{f}_{t_{1,2}} \,, \end{cases} \tag{13}$$

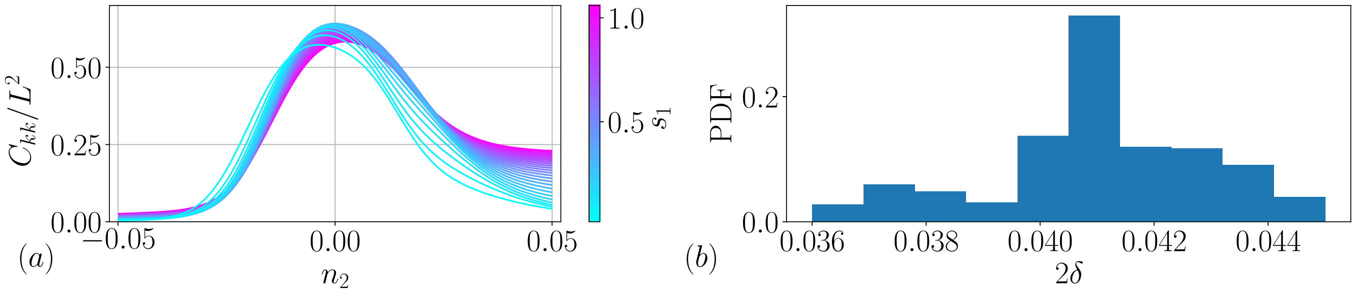

FIG. S2: (a) Profiles of polymer extension $C_{kk}(s_1, n_2)/L^2$ at various locations s_1, the curvilinear coordinate along the stressline $\boldsymbol{\mathcal{T}}_{1,\max}$ passing through the point of global maximum extension of the arrowhead, and as function of n_2, the coordinate on a line locally perpendicular to the stressline. The profiles are colored by s_1 along the sheet. For reference from Fig. 2(a) of the manuscript, $s_1 = 0$ is $x = 0$ and $s_1 = 1$ is $x \approx -\pi$. (b) Probability density function (PDF) of the thickness 2δ of the sheet measured from the two locations of each profile where $C_{kk}(s_1, n_2) = \max_{n_2}(C_{kk}(s_1, n_2)/2$. 1000 profiles from $0 \le s_1 \le 1$ are used for the PDF. The mean value is 0.041.

where $\mathbf{E} = \frac{1}{2}\left(\boldsymbol{\nabla}\mathbf{u} + \boldsymbol{\nabla}\mathbf{u}^{\mathrm{T}}\right)$ is the strain rate tensor. Finally, making the assumption that the interface is aligned with a stressline $\boldsymbol{\mathcal{T}}_1$, we can replace $\mathbf{n}$ by $\mathbf{e}^{(2)}$. Furthermore, in the present two-dimensional case only one tangent vector, denoted $\mathbf{t}$, exists and can thus be replaced by $\mathbf{e}^{(1)}$.

As a last step, we can use Eq. (5) of the main text to express the surface force $\tilde{\mathbf{f}}$ as the polymer body force integrated over the sheet thickness:

$$-\tilde{f}_n \approx \frac{1-\beta}{Re} \int_{-\delta}^{+\delta} \left(\tilde{\partial}_2 \tau_2 + \kappa_1 N_1\right) \mathrm{d}n_2 \tag{14}$$

$$-\tilde{f}_t \approx \frac{1-\beta}{Re} \int_{-\delta}^{+\delta} \left(\tilde{\partial}_1 \tau_1 - \kappa_2 N_1\right) \mathrm{d}n_2 \tag{15}$$

where n_2 is a local coordinate normal to the sheet, and 2δ is a characteristic thickness of the sheet.

As illustrated in Fig. 4(b) of the main text, in some regions the tangential component of the polymer body force is organized in two layers and pointing in opposite directions, thus creating a torque in the sheet. These two layers can also be modeled as a single interface by introducing a surface torque distribution

$$\Gamma \approx \frac{1-\beta}{Re} \int_{-\delta}^{+\delta} \left(\tilde{\partial}_1 \tau_1 - \kappa_2 N_1\right) n_2 \, \mathrm{d}n_2 \,, \tag{16}$$

where the origin of n_2 is taken at the interface. This surface torque distribution induces a discontinuity of the tangential velocity across the interface that is proportional to Γ.

The definition of polymer extension sheet remains an open question for future studies. Here we chose to define the sheet's skeleton as the stressline passing through the point of global maximum extension, $\boldsymbol{\mathcal{T}}_{1,\max}$, indicated by the thicker green line in Figs. 3 and 4(a-b) of the main text. On this stressline, the curvilinear coordinate is defined as s_1. The analysis of the sheet thickness is confined to the arrowhead part, since this is the most relevant to our discussion. The head of the arrowhead is located at $s_1 = 0$, corresponding to $x \approx 0$ in all the figures of the manuscript. The sheet thickness is investigated over the interval $0 \le s_1 \le 1$, which includes the global maximum of polymer extension at $s_1 \approx 0.3$. Fig. S2(a) shows 40 out of 1000 samples of cross-sectional profiles over $0 \le s_1 \le 1$. As it can be observed in Fig. 4 of the main text, the chosen stressline $\boldsymbol{\mathcal{T}}_{1,\max}$ follows closely the maximum polymer extension in most cross-sections of the arrowhead sheet. At any location s_1, the sheet thickness 2δ is defined by the width between the two points where the polymer extension is half the maximum extension in that cross-section. The probability density distribution of these 1000 thicknesses is compiled in Fig. S2(b), which shows a consistent width with a mean of $2\delta = 0.041$.

Adopting a thickness of 0.04, we compare in Fig. S3 the evolution along $\boldsymbol{\mathcal{T}}_{1,\max}$ of the pressure jump, $\Delta P_\perp = p_{\mathrm{II}} - p_{\mathrm{I}}$, and the jump of strain rate $\Delta E_\perp$, i.e., the first and second terms on the LHS of Eq. (6) in the main text, and the RHS of the same equation. The RHS is the integral across the thickness of the sheet of f_2, which is the sum of the contributions of $\tilde{\partial}_2 \tau_2$, the gradient of the second eigenvalue along the direction defined by the second eigenvector, and the curvature of the sheet multiplied by the local first normal stress difference, as also given by Eq. (14). For context, the maximum root-mean-squared of pressure in planes parallel to the wall is about 10^{-3}. The pressure

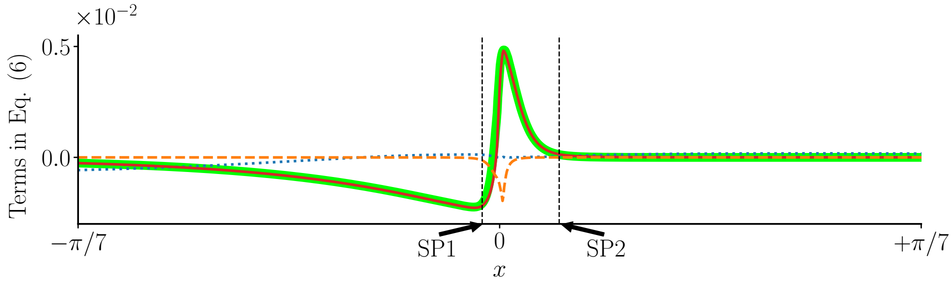

FIG. S3: Comparison between the different terms of Eq. (6) in the main text: pressure jump $\Delta P_{\perp} = p_{\rm II} - p_{\rm I}$ (green line) and strain rate jump $\Delta E_{\perp}$ (blue dotted line) across the stress polymer sheet centered on the stressline $\boldsymbol{\mathcal{T}}_{1,\max}$, polymer body force component integrated over the thickness of the sheet $-\tilde{f}_n = \int_{-\delta}^{+\delta} f_2 \, \mathrm{d}n_2$ (red line), and contribution of $\tilde{\partial}_2 \tau_2$ to $-\tilde{f}_n$ (orange dashed line). The evolutions of these quantities along $\boldsymbol{\mathcal{T}}_{1,\max}$ is plotted as a function of the horizontal location x for direct correspondence with Fig. 4 in the main text. The thickness of the sheet is 2δ, $\delta = 0.04$.

jump $\Delta P_{\perp} = p_{\rm II} - p_{\rm I}$ shown in Fig. S3 is seven times higher. Figure S3 shows first that the contribution of the strain rate jump is negligible along most of the sheet. More importantly, we can observed an excellent agreement between the pressure jump and the integral of the forcing term. Except around $x = 0$, between the zones of maximum and minimum pressure where the stressline abruptly changes direction, the contribution of $\tilde{\partial}_2 \tau_2$ is negligible, i.e., $-\tilde{f}_n \approx \int_{-\delta}^{+\delta} f_2 \, \mathrm{d}n_2 \approx (1-\beta)/Re \int_{-\delta}^{+\delta} \kappa_1 N_1 \, \mathrm{d}n_2$. In other words, in most of the curved part of the arrowhead, the term $\kappa_1 N_1$ appears to drive the pressure jump $\Delta P_{\perp}$. This demonstrates that the pressure jump across a curved sheet of high polymer stress can be very well approximated by the sheet curvature and the associated first normal stress difference. Finally, note that the agreement shown in Fig. S3 improves for $2\delta < 0.04$ and marginally degrades when $2\delta = 0.1$ (not shown).

The present flow is not found to produce large enough principal polymer stress variation $\tilde{\partial}_1 \tau_1$ along the stressline to create an observable shear rate jump across the sheet. The validation of Eq. (7) in the main text will thus require future studies in different flows, especially flows with significant $\tilde{\partial}_1 \tau_1$, like plumes of convection cells (see for instance Fig. 1 in reference [3] where the polymer stress causes significant velocity deficit at the center of the vertical plumes).

Equations (6) and (7) in the main text illustrate the possible parallels that may exist between EIT-type flows and interfacial flows, however much work is needed to refine the definition of polymer stress sheets, their thickness, and the regimes where each equation is a satisfactory approximation of the dynamics.

[1] K. J. Burns, G. M. Vasil, J. S. Oishi, D. Lecoanet, and B. P. Brown, Dedalus: A flexible framework for numerical simulations with spectral methods, Physical Review Research **2** (2020).
[2] M. P. do Carmo, *Differential geometry of curves and surfaces* (Dover Publications, 2016).
[3] Y. Dubief and V. E. Terrapon, Heat transfer enhancement and reduction in low-Rayleigh number natural convection flow with polymer additives, Physics of Fluids **32** (2020).